THE ^{95}Zr BRANCH

$^{95}Zr \rightarrow {}^{96}Zr$

OR

$\rightarrow {}^{95}Mo$

ALSO ^{93}Zr

ZrO NEEDED

S STARS AND NOT 'ALL' PHASES

A =	90	91	92	93	94	95
σ =	19.4	60	33	95	26	79

96

10.7

TABLE 2

ISOTOPIC ZIRCONIUM ABUNDANCES

				$^{i}Zr/Zr$ (per cent)					
Star	Sp. Type	Mode[a]	System i =	90	91	92	93	94	96
R And	S6,6e	E	B–X	32	18	14	7	14	< 5
		E	γ	40	12	21	4	22	< 2
		G	B–X	36	11	14	7	30	< 2
BI And	S8,8	G	B–X	48	14	15	4	16	< 3
T Cam	S4,7e	E	B–X	34	18	13	11	19	< 2
		E	γ	38	15	17	6	20	< 2
S Cas	S4,6e	G	B–X	49	11	16	3	16	< 5
U Cas	S5,5e	G	B–X	44	10	20	9	14	< 3
AD Cyg	S5,8	E	B–X	30	16	16	14	23	< 2
		E	γ	35	15	20	7	21	< 2
R Gem	S3,9e	E	B–X	35	20	13	3	25	< 4

[a] E ≡ echelle and G ≡ grating (see text).

"STABLE" in s-process TP plane

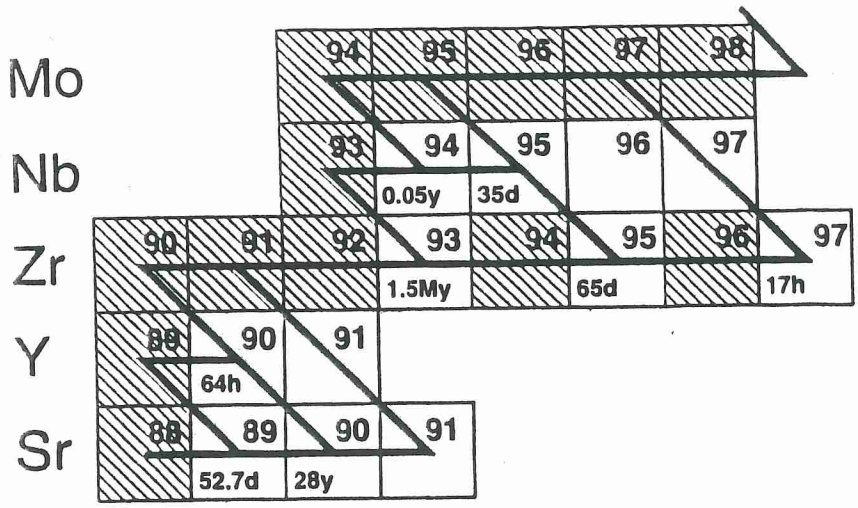

FIG. 9.—*s*-process path from Sr to Mo for neutron densities of 10^{10} cm^{-3} or less. Stable nuclei are represented by a striped box and unstable nuclei an open box in which the half life may be given—the half life of ^{94}Nb is quite temperature sensitive and the value for $T = 2 \times 10^8$ K is given. Major branches are given for neutron densities $N(n) \lesssim 10^{10}$ cm^{-3}.

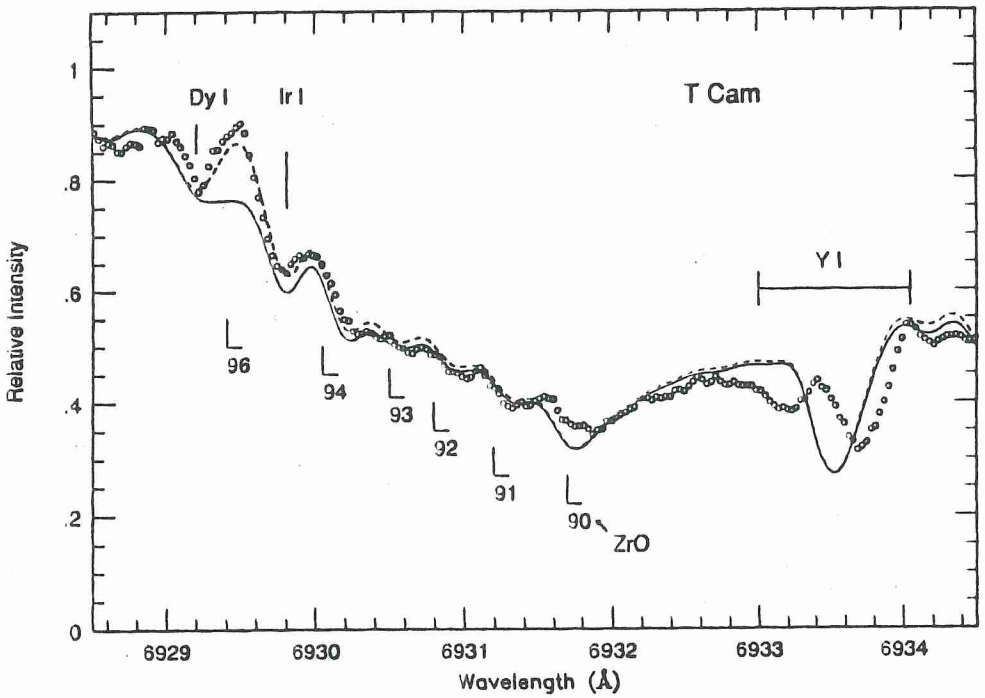

FIG. 7.—Observed (*filled circles*) and sample ZrO synthetic spectra for the S star T Cam. The $B-X$ 0–1 bandheads are synthesized for two difference isotropic mixtures of Zr: the solid line is a synthesis with no ^{96}ZrO in the mixture, while the dashed line contains a fractional content of 0.04 ^{96}Zr. The two atomic absorption lines near the ^{96}ZrO bandhead are noted (Dy I and Ir I) and illustrate the need for care in examining and synthesizing the S stars. Clearly, no absorption from ^{96}ZrO is indicated to a rather small fraction, i.e., $f \lesssim 0.02$. In addition, we note the complicated feature near in the observed spectrum near the expected position of a low-lying (0.05 eV) Y I line. In many of the S stars, this line changes shape and position and we suspect that circumstellar absorption and emission may contaminate this line.

$^{93}Zr \rightarrow {}^{93}Nb$

- CLOCK SINCE END OF S-PROCESSING
- BaII JCap (MASS TRANSFER)

  Smith & Lambert (1984, ApJ 96, 226)

- $^{93}Nb \simeq {}^{93}Zr$ (s)

  ^{93}Zr / all Zr ⇒ THERMOMETER

  Neyskens et al. (Nature, 2015, 517, 174)

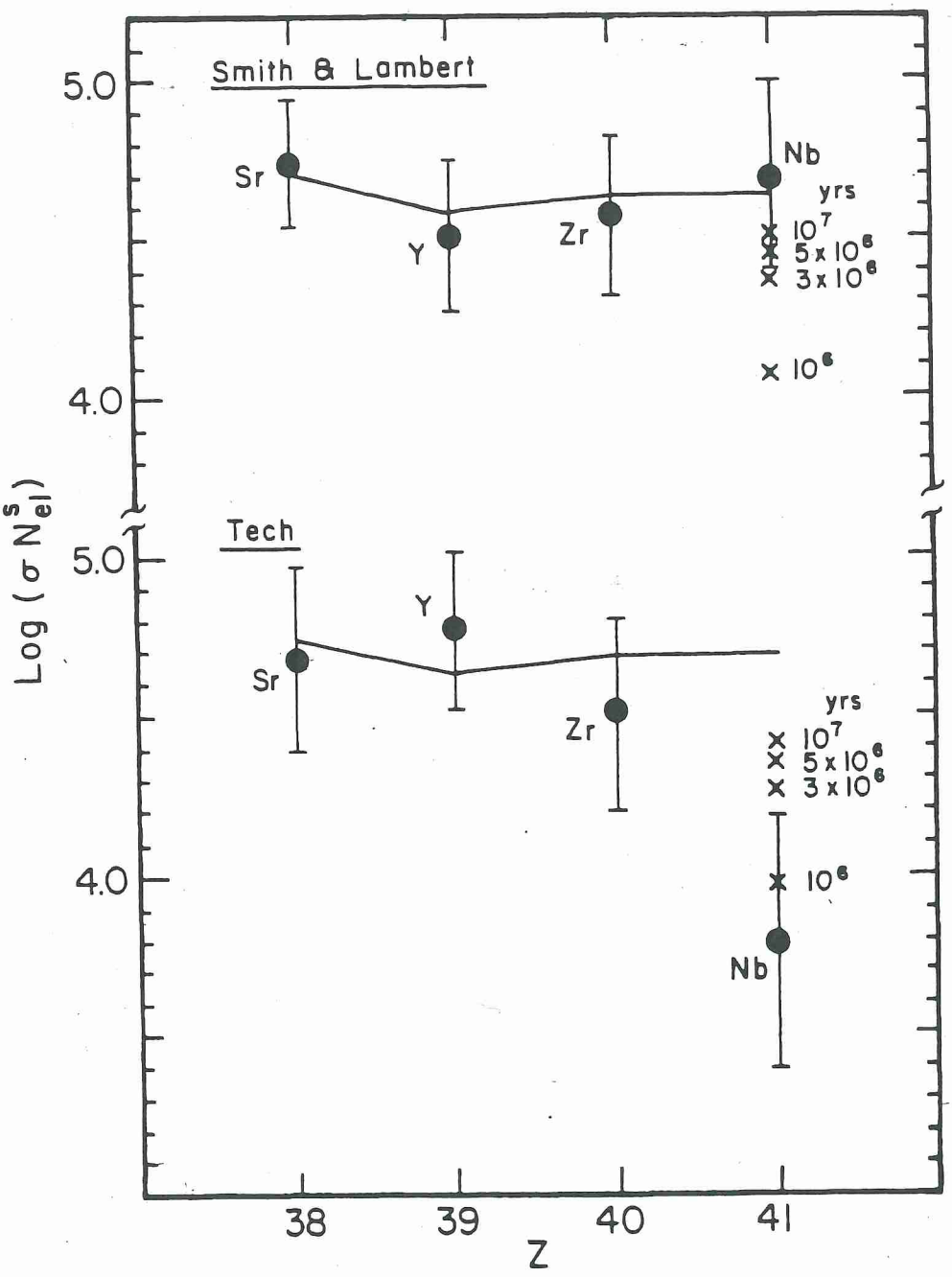

FIG. 3—Log (σN_{el}^{s}) for elements near Nb in ζ Cap from this study and that of Tech (1971). The solid circles with error estimates are the observations; the solid line is a model prediction (Cowley and Downs 1980) with $\tau_0 = 0.3$. The crosses show the expected values for Nb at several times after the end of *s*-processing, based upon the observed zirconium abundances and an equilibrium *s*-process abundance ratio of $\log \epsilon(^{93}\mathrm{Zr}) - \log \epsilon(\mathrm{Zr}_{\mathrm{total}}) = -1.15$.

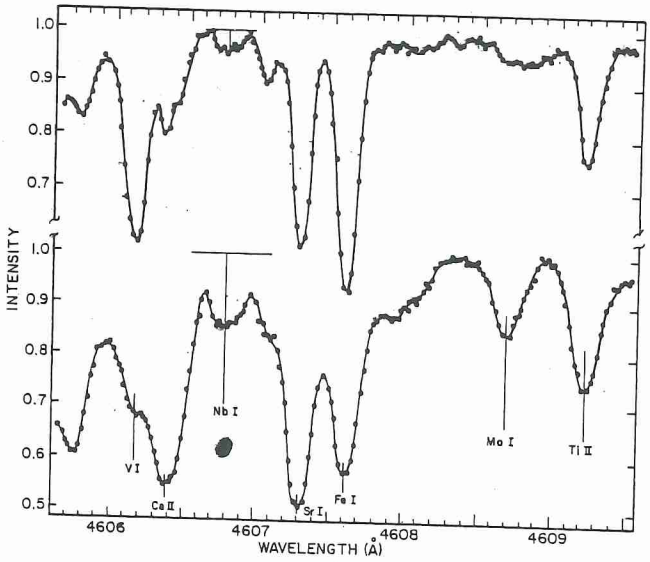

FIG. 1—Spectra of ϵ Vir (top) and ζ Cap (bottom) near the λ4606.8 Å Nb I line. The continuum placement at the Nb I line is shown in each spectrum.

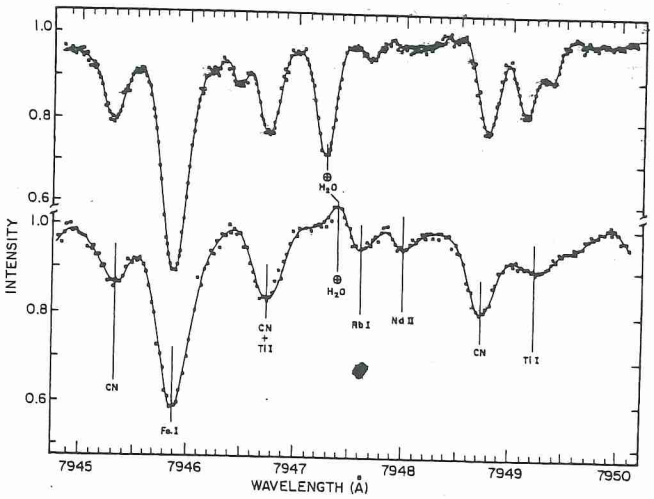

FIG. 2—Spectra of ϵ Vir (top) and ζ Cap (bottom) near the λ7947.6 Å Rb I line. Note the residual H_2O feature just to the short-wavelength side of the Rb I line caused by division of the spectrum by a hot-star spectrum (α PsA).

Nb I

Rb I

s-process : THERMOMETER & CHRONOMETER

- $^{93}Zr \rightarrow {}^{93}Nb$ after s-processing
  - ^{93}Nb: SOLE ISOTOPE

$$^{93}Zr / \sum_i {}^{i}Zr \equiv {}^{93}Nb / \sum {}^{i}Zr$$

= THERMOMETER

NEYSKENS et al. 2015 Nature 517, 174

- S STARS
  - INTRINSIC T_c ✓
  - EXTRINSIC T_c X

REMINDER! AGB SPECTRA ARE RIDDLED WITH LINES

∴ ANALYSE BA STARS

astro-ph 1604.03031

182 Ba stars!

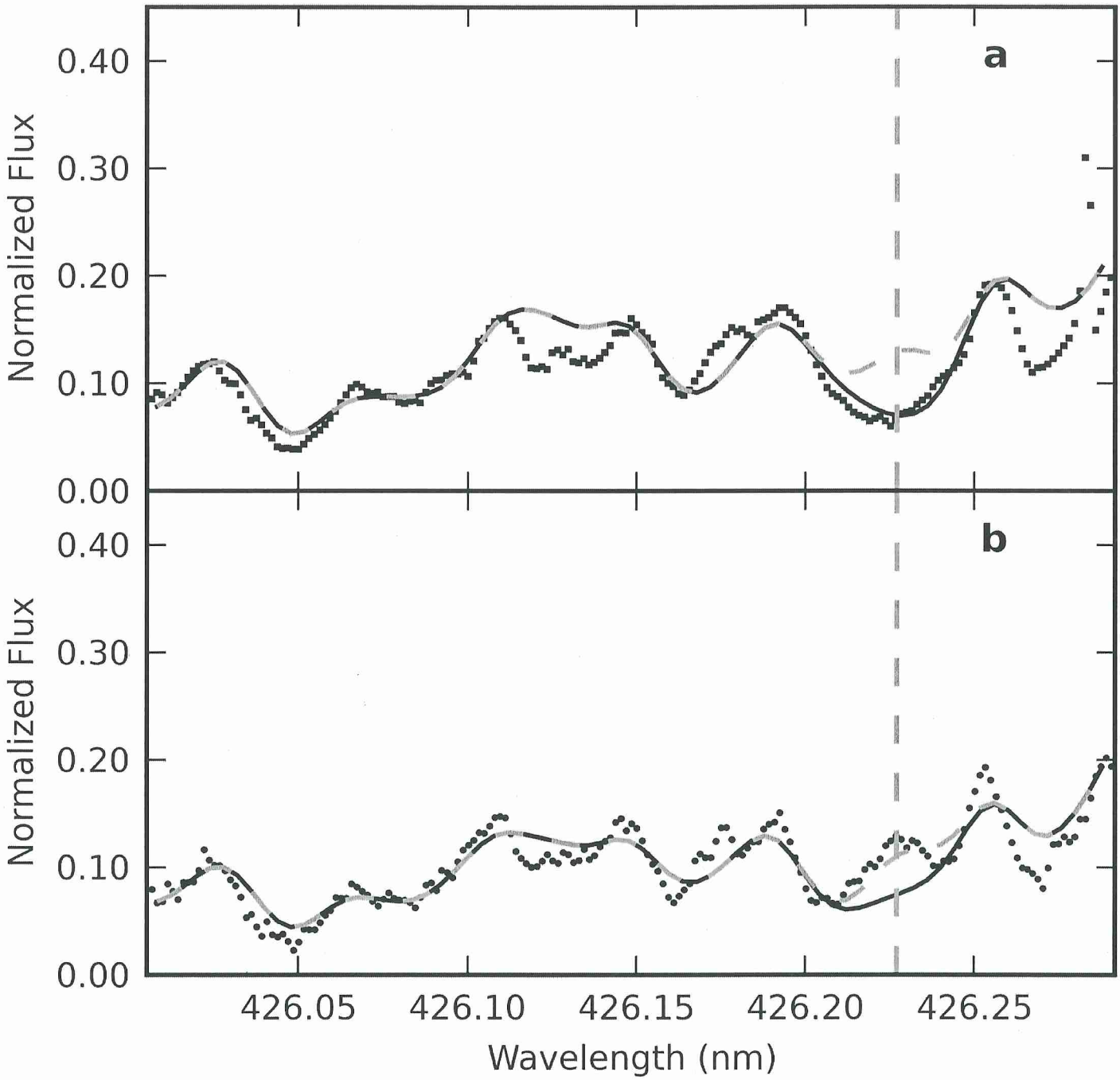
a
b
Normalized Flux
Normalized Flux
0.40
0.30
0.20
0.10
0.00
0.40
0.30
0.20
0.10
0.00
426.05
426.10
426.15
426.20
426.25
Wavelength (nm)

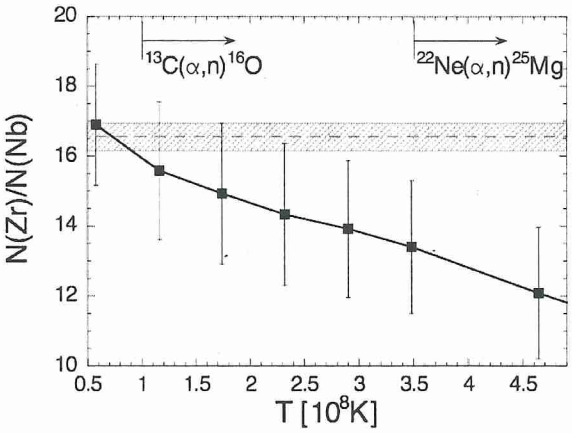
20
18
16
14
12
10
N(Zr)/N(Nb)
$^{13}C(\alpha,n)^{16}O$
$^{22}Ne(\alpha,n)^{25}Mg$
0.5
1
1.5
2
2.5
3
3.5
4
4.5
T [10^8K]

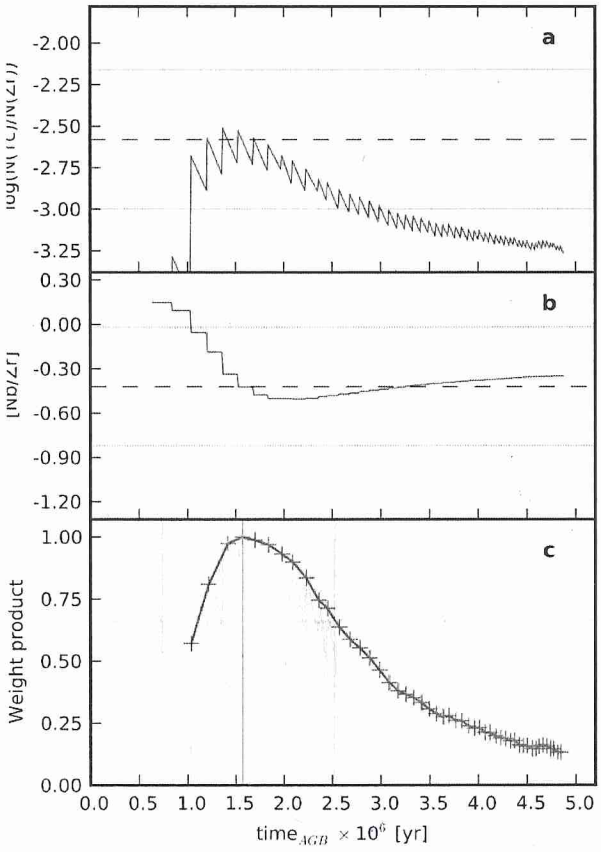
a
b
c
-2.00
-2.25
-2.50
-2.75
-3.00
-3.25
0.30
0.00
-0.30
-0.60
-0.90
-1.20
1.00
0.75
0.50
0.25
0.00
Weight product
0.0
0.5
1.0
1.5
2.0
2.5
3.0
3.5
4.0
4.5
5.0
time$_{AGB}$ × 10^6 [yr]

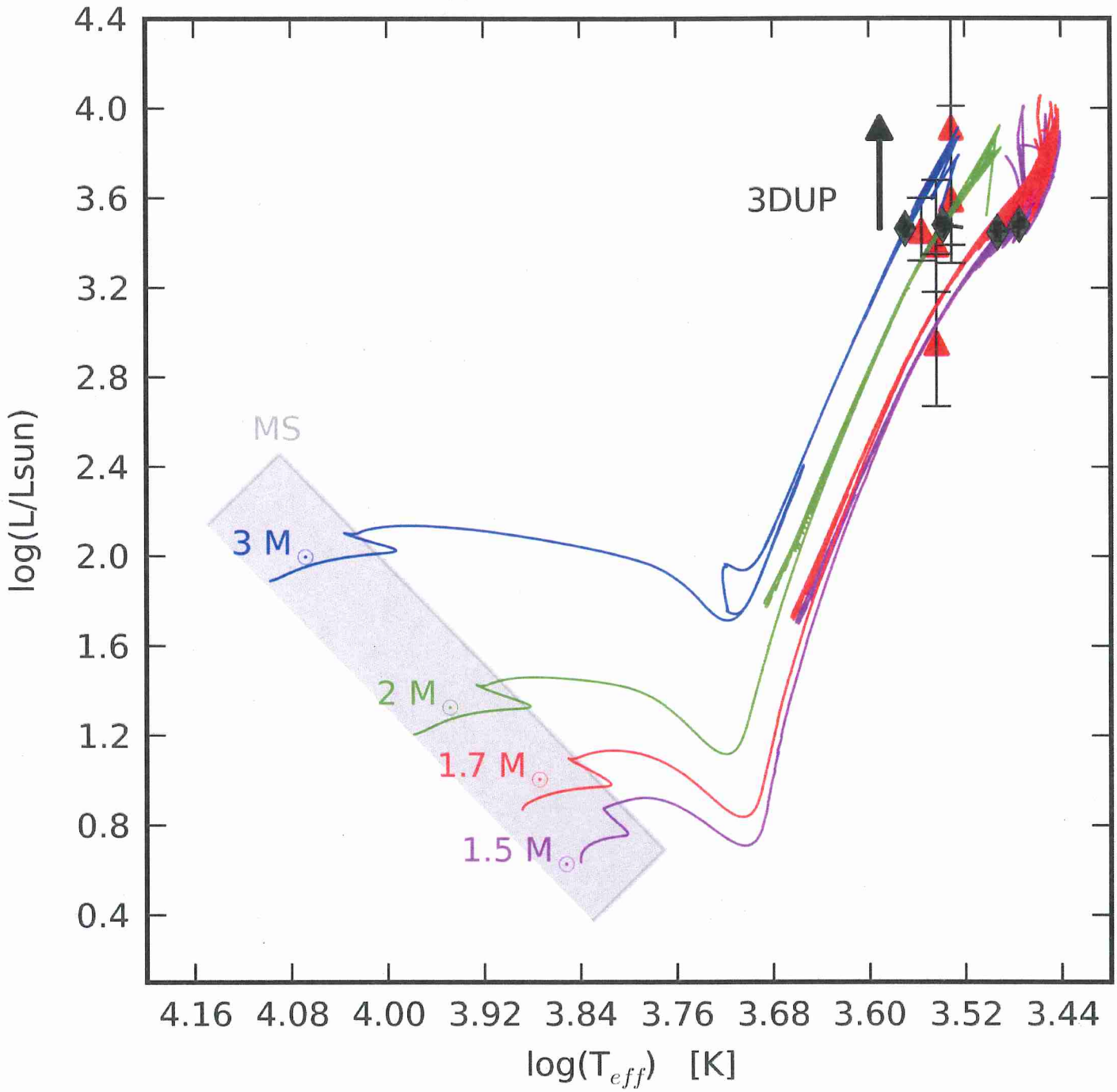
4.4
4.0
3.6
3.2
2.8
2.4
2.0
1.6
1.2
0.8
0.4
log(L/Lsun)
4.16
4.08
4.00
3.92
3.84
3.76
3.68
3.60
3.52
3.44
log(T_eff) [K]
3DUP
MS
3 M⊙
2 M⊙
1.7 M⊙
1.5 M⊙

λ_{pm} 2% – 30%

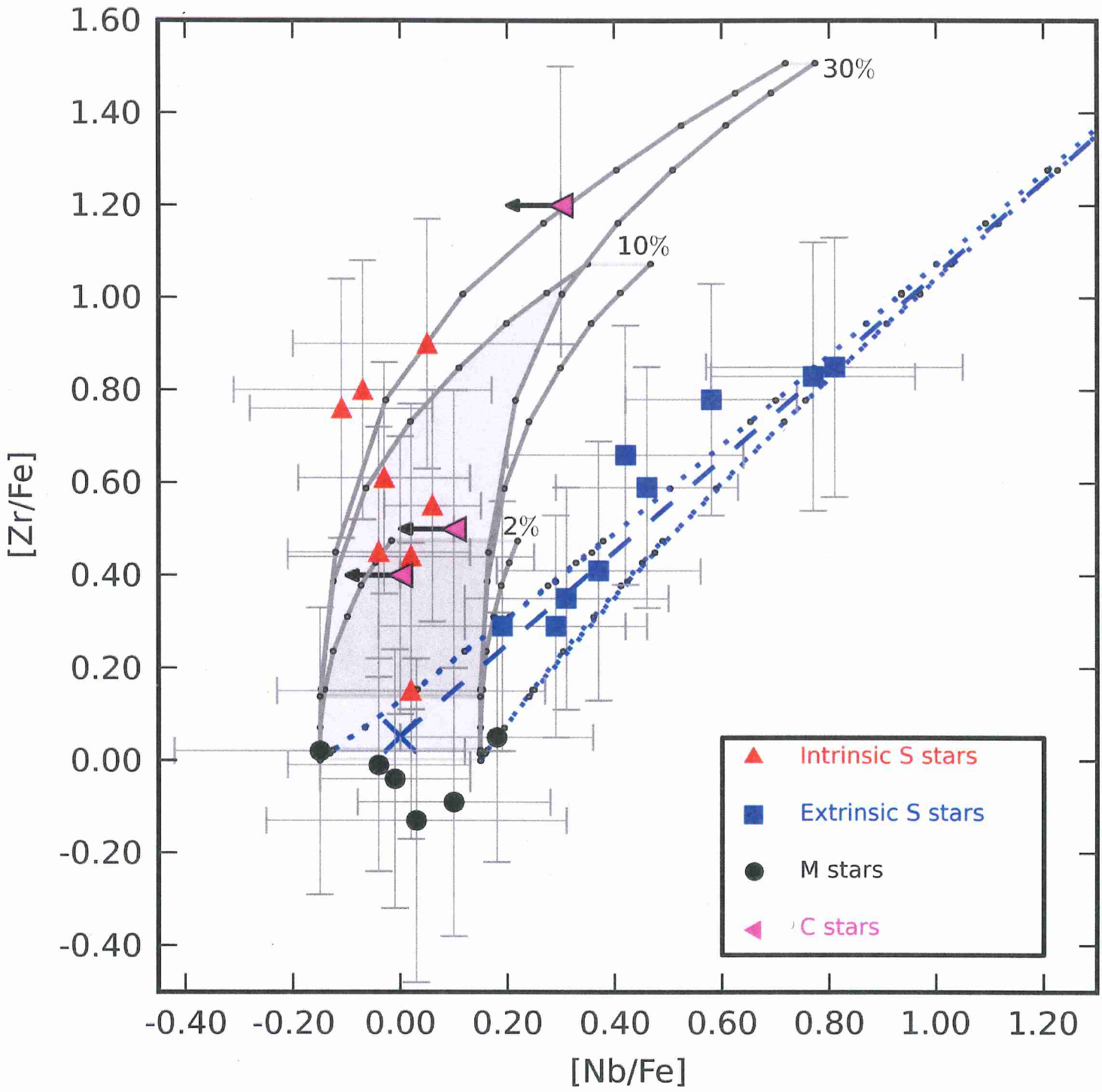

ANOTHER 'STELLAR' BRANCH in the S-PROCESS FLOW

$^{151}Sm \rightarrow {}^{151}Eu$ vs ^{153}Eu

& ISOTOPIC FRACTIONS

- ^{151}Sm $\tau_{1/2} \sim f(T)$

  $= 93$ yrs (COLD

  $\div 30$ at the interstellar T

- BRANCHING AFFECTS $^{151}Eu/^{153}Eu$

  BUT Eu primarily r-process

  - test r-process ✓
  - test s-process is s↑ ?

- Eu II lines have hfs AND isotopic shift

  Can measure iso ratio at high spectral res.

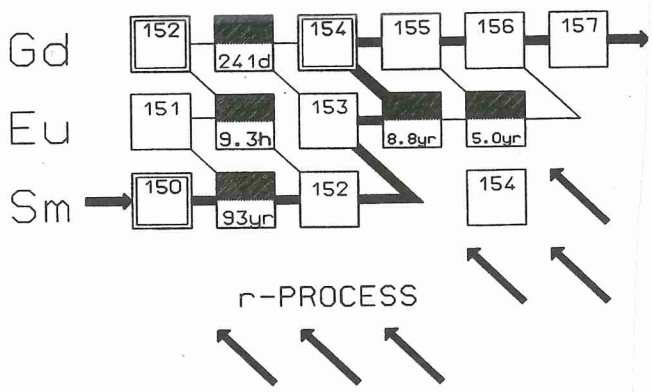

FIG. 1. The *s*-process path in the region of the gadolinium isotopes.

151 Sm 0 keV 90 yr β^- 100%

261.13 keV 1.4 μs π 100%

effective $\tau_{1/2}$ as function of temperature

Fig. 1 CITED IN TEXT | HIGH-RESOLUTION IMAGE (170kb) |

Comparison of the observed spectra (*filled circles*) and synthetic spectra (*lines*) for the Eu II 4129 Å line. e name of the object and the adopted fr(^{151}Eu) value are given in each panel. The solid line shows the synthetic spectra for the adopted fr(^{151}Eu); the dotted and dashed lines show those for ratios that are smaller and larger by 0.15 in fr(^{151}Eu), respectively. The wavelengths and relative strength of the hyperfine components for ^{151}Eu and ^{153}Eu are shown in the top panel.

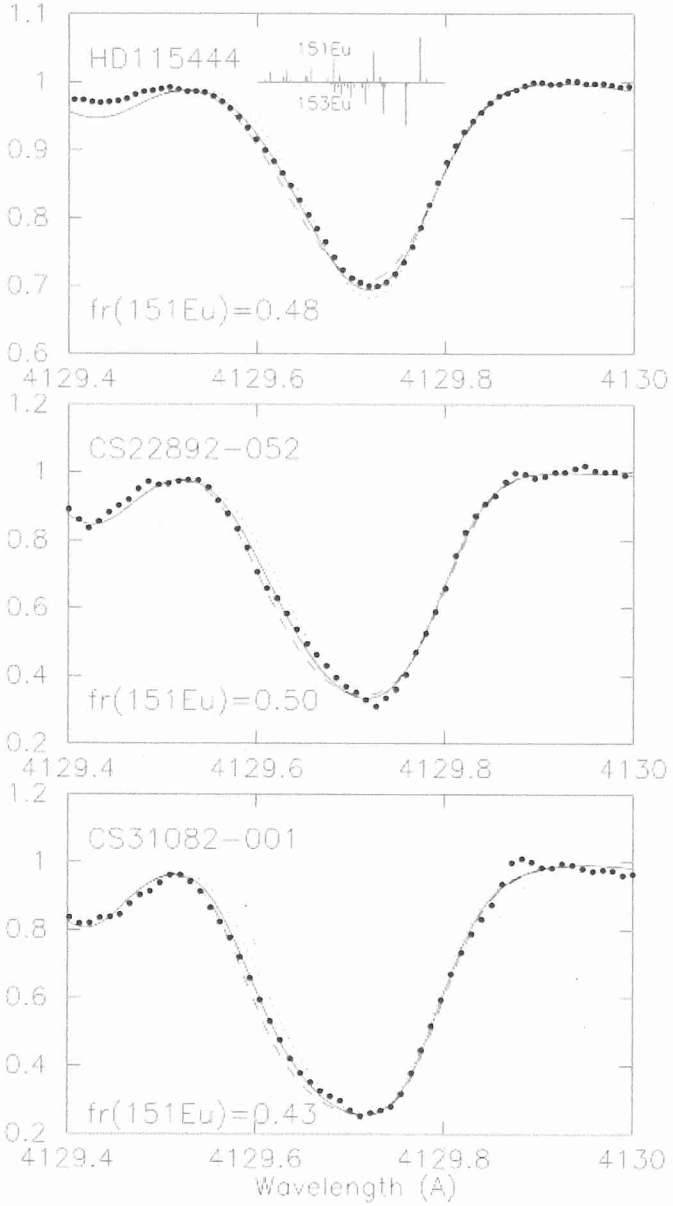

Aoki et al.
2003, ApJ 586 506
these are
r-process enriched
stars

See also Sneden et al.
2002, ApJ 566 L25

Fig. 2

CITED IN TEXT | HIGH-RESOLUTION IMAGE (103kb) |

Same as Fig. 1, but for the Eu II 4435 Å line

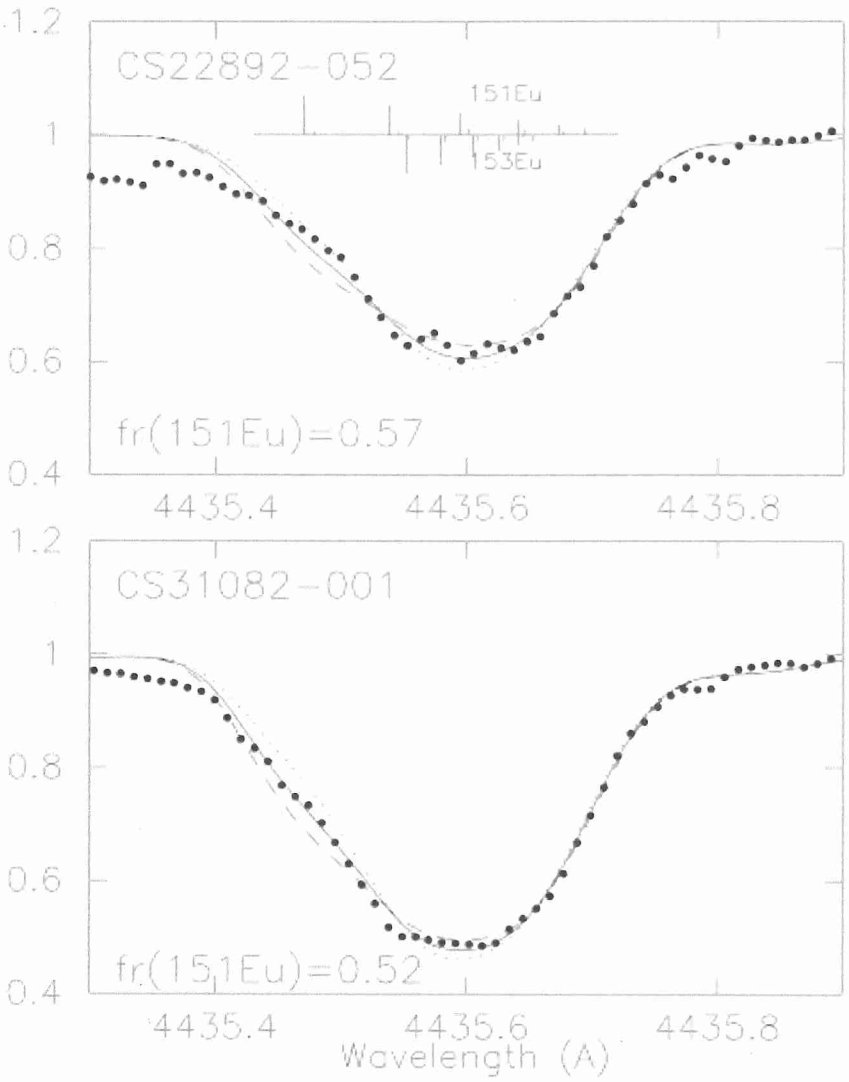

Aoki et al. (2003)

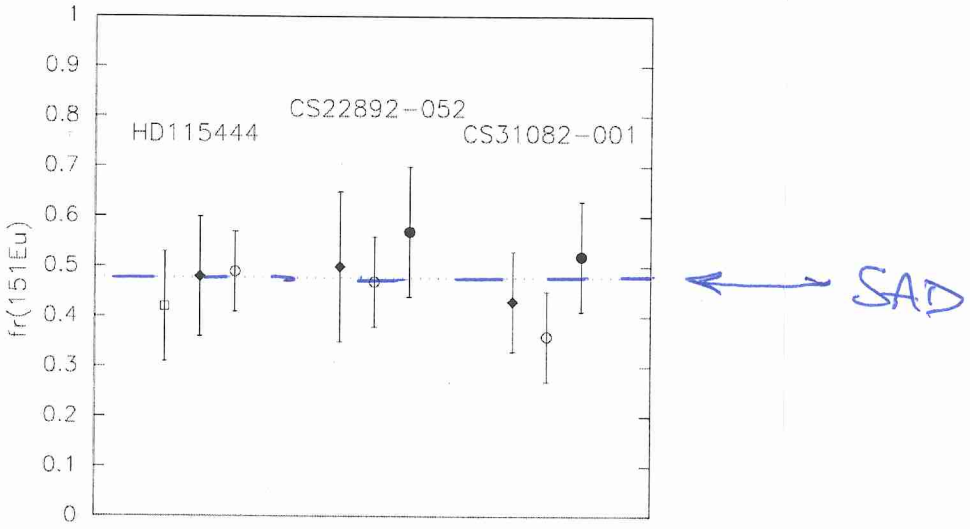

FIG. 4.—Results of the ^{151}Eu fractions and uncertainties (σ_{total}). The results obtained by consideration of Eu II 3819, 4129, 4205, and 4435 Å are shown by squares, diamonds, open circles, and filled circles, respectively. The dotted line is the ^{151}Eu fraction in solar system material (0.478). Note that the isotopic fractions derived for all three lines considered for CS 31082-001 are lower than those obtained for CS 22892-052, although the error bars overlap.

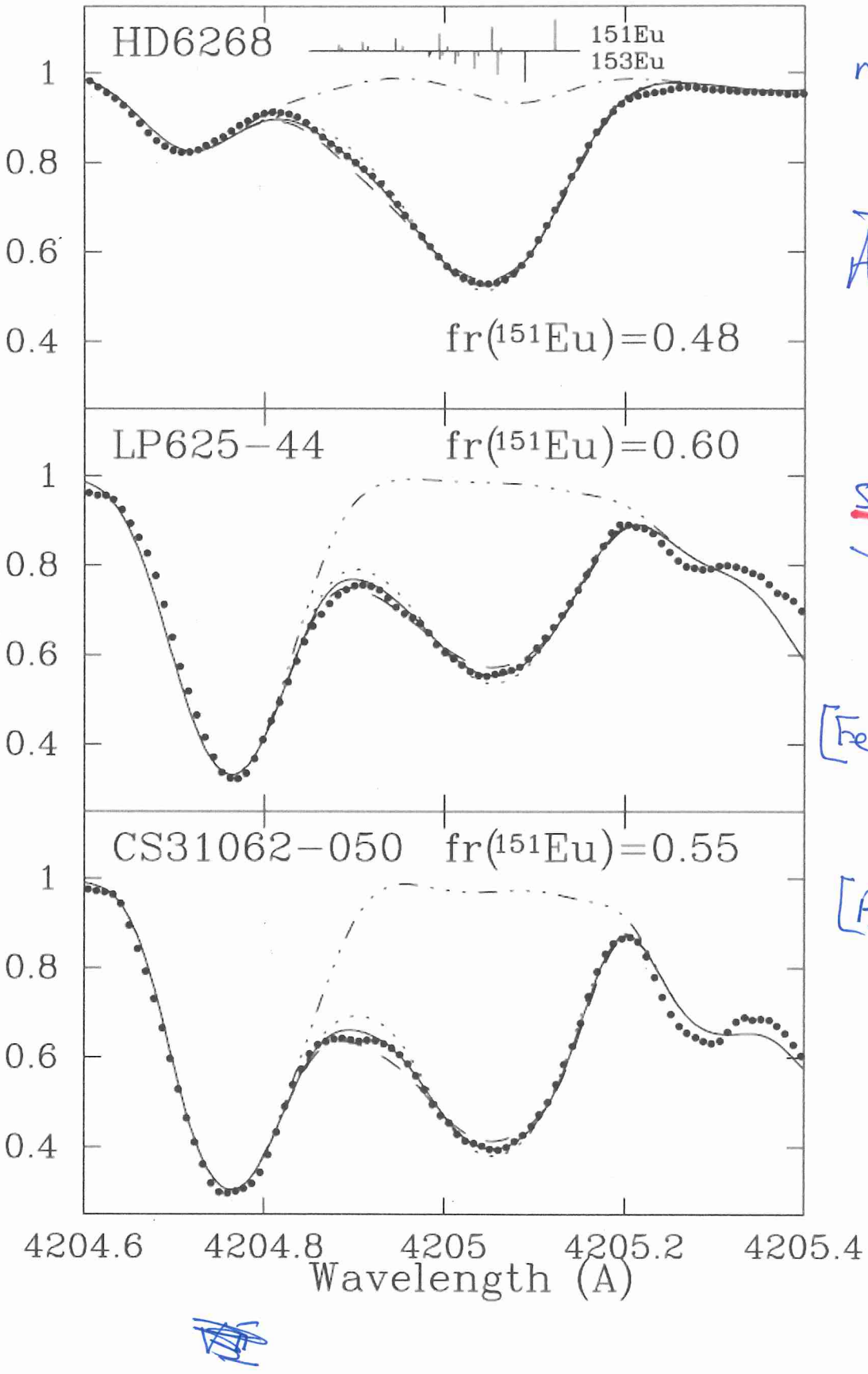

mol. r

−2.5

Aoki et al. 2003 ApJ L67

s-process enhanced

[Fe II/I] = −2.7

[Ba/Fe] = +2.5

−2.4

Fig. 1

CITED IN TEXT | HIGH-RESOLUTION IMAGE (230kb) |

Comparison of the observed spectra (*filled circles*) and synthetic ones (*lines*) for the Eu II 4205 Å line. The name of the object and the adopted fr(^{151}Eu) value are presented in each panel. The solid line shows the synthetic spectra for the adopted fr(^{151}Eu); the dotted and dashed lines show those for ratios that are smaller and larger by 0.10 in fr(^{151}Eu), respectively. The dot-dashed lines show the synthetic spectra for no Eu. The weak blending at 4205.09 Å in the spectrum of HD 6268 (*top*) is due to V II, whose effect is negligible in the two subgiants. The wavelengths and relative strength of the hyperfine components for ^{151}Eu and ^{153}Eu are shown in the top panel.

TABLE 2

RESULTS

	HD 6268		LP 625−44		CS 31062−050	
LINE	fr(^{151}Eu)	log ϵ(Eu)	fr(^{151}Eu)	log ϵ(Eu)	fr(^{151}Eu)	log ϵ(Eu)
λ3819	0.44 ± 0.11	−1.55	0.68 ± 0.10	−0.44	0.65 ± 0.14	−0.02
λ4129	0.49 ± 0.07	−1.57	0.56 ± 0.07	−0.45	0.56 ± 0.09	+0.01
λ4205	0.48 ± 0.04	−1.54	0.60 ± 0.06	−0.43	0.55 ± 0.05	+0.04

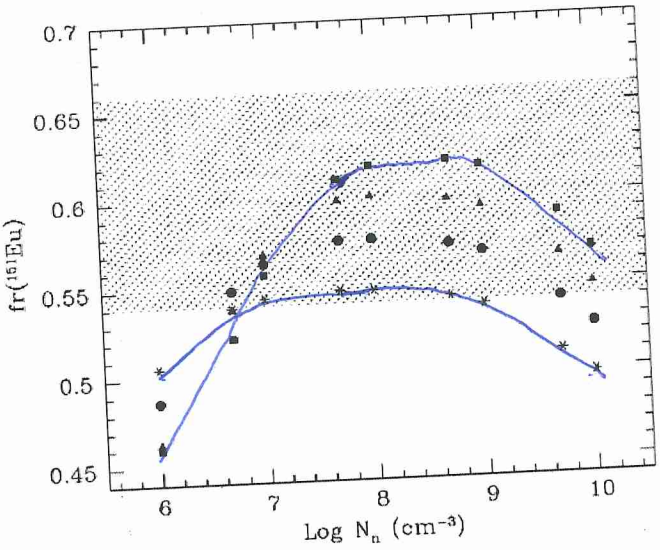

FIG. 2.—The fr(^{151}Eu) values calculated for four temperatures (*squares*: kT = 30 keV; *triangles*: 20 keV; *circles*: 15 keV; *asterisks*: 10 keV) as a function of neutron density (N_n). The fr(^{151}Eu) of LP 625−44 and its uncertainty is shown by the hatched area.

Figure 4. CITED IN TEXT | HIGH RESOLUTION IMAGE Go to: Figure 3. | Figure 5.

Our synthesis of the Eu II line at 4129 Å in HD 175305. We have measured an isotopic fraction of $f_{151} = 0.50 \pm 0.04$ for this line. The observed spectrum is indicated by open squares. In panel *a*, we show the syntheses with the extreme values of f_{151} as well as the pure-*s* and pure-*r*-process syntheses. In panel *b*, the solid curve represents our best-fit isotopic fraction, while the dotted curves represent the 3 σ uncertainties. In both panels, the long-dashed curve is a synthesis with no Eu present, indicating that this line is generally free of blending features. The vertical lines represent the positions and relative strengths of the individual hyperfine components; dotted lines represent ^{151}Eu, while solid lines represent ^{153}Eu. Note that the Eu elemental abundance reported is the best-fit value for this synthesis and not our derived Eu abundance for HD 175305.

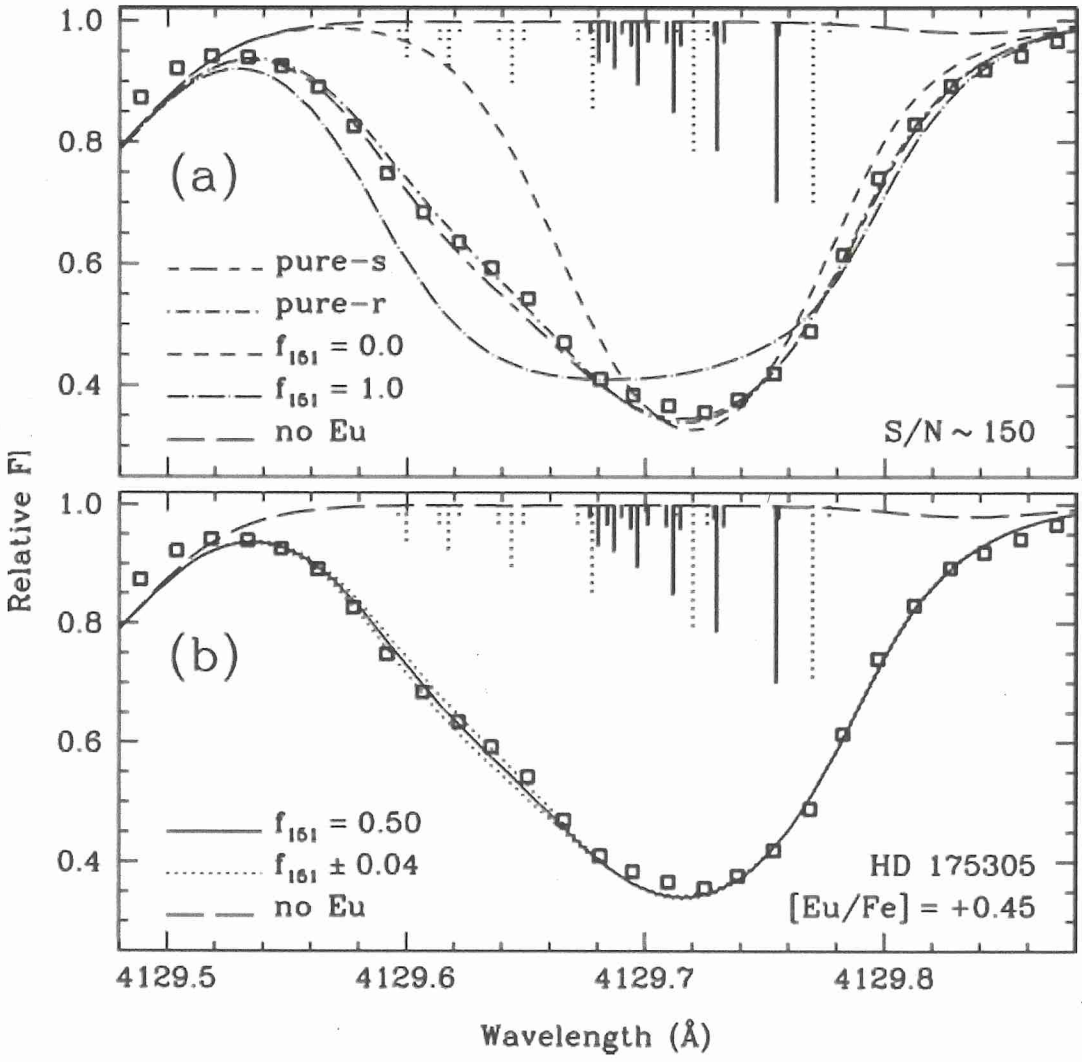

Roederer et al. 2008 ApJ 675, 723

Figure 7. CITED IN TEXT | HIGH RESOLUTION IMAGE Go to: Figure 6. | Figure 8.

Our synthesis of the Eu II line at 4435 Å in HD 175305. Symbols are the same as in Fig. 4. We emphasize that the isotopic fraction shown in panel *b* is the value derived from the 4129 Å line and not a fit to this line. Note the strong blend with the saturated Ca I line at 4535.67 Å. The isotope fraction derived from the 4129 Å line provides a reasonable fit to the 4435 Å line as well, requiring only small changes in the elemental abundance.

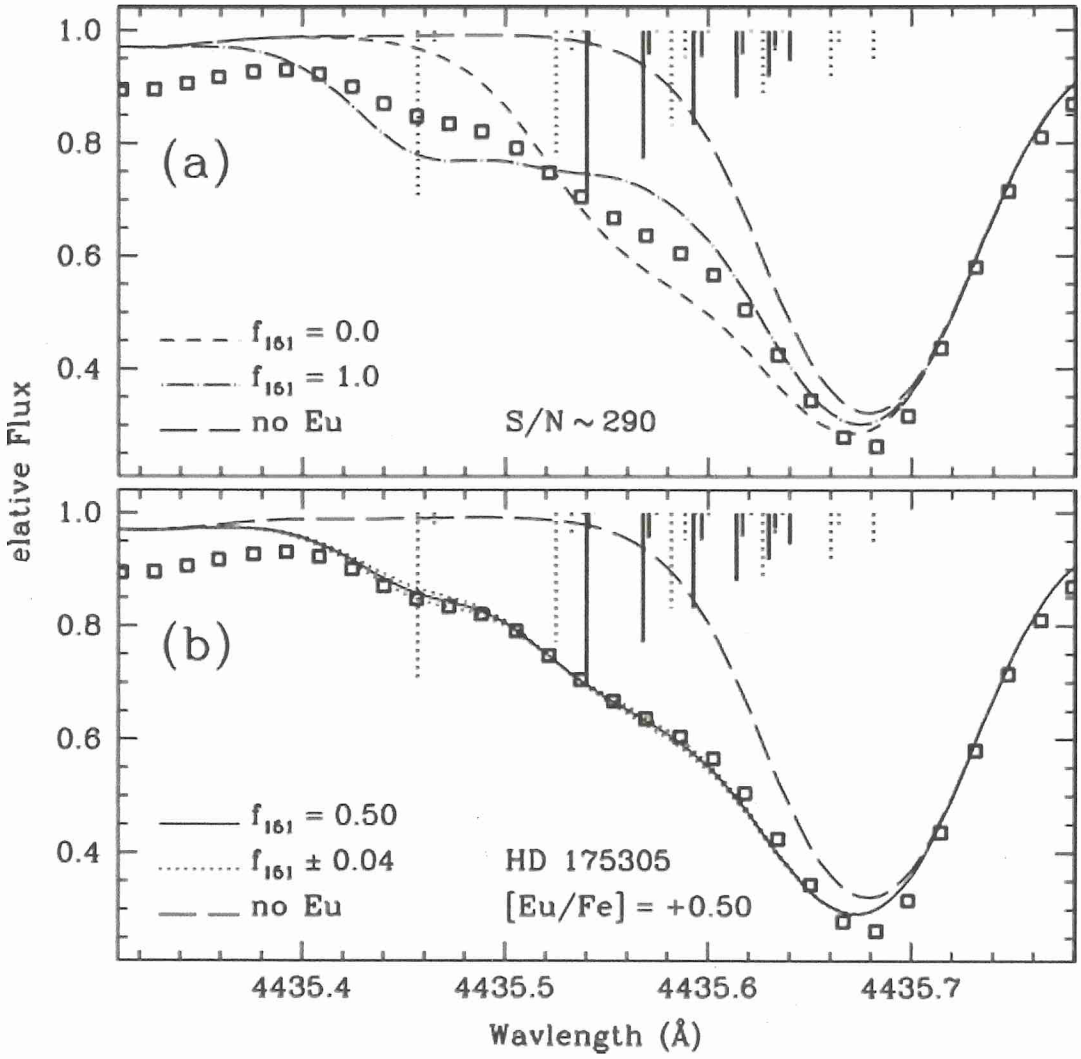

TP-AGB models replace CLASSICAL APPROACH.

- n from ^{13}C pocket: $^{13}C(\alpha,n)^{16}O$
- n also from the conv. episode $^{13}C(\alpha,n)^{16}O + {}^{22}Ne(\alpha,n)^{25}Mg$

→ **MODEL** ^{13}C POCKET ('free' parameter)

FIG. 10.

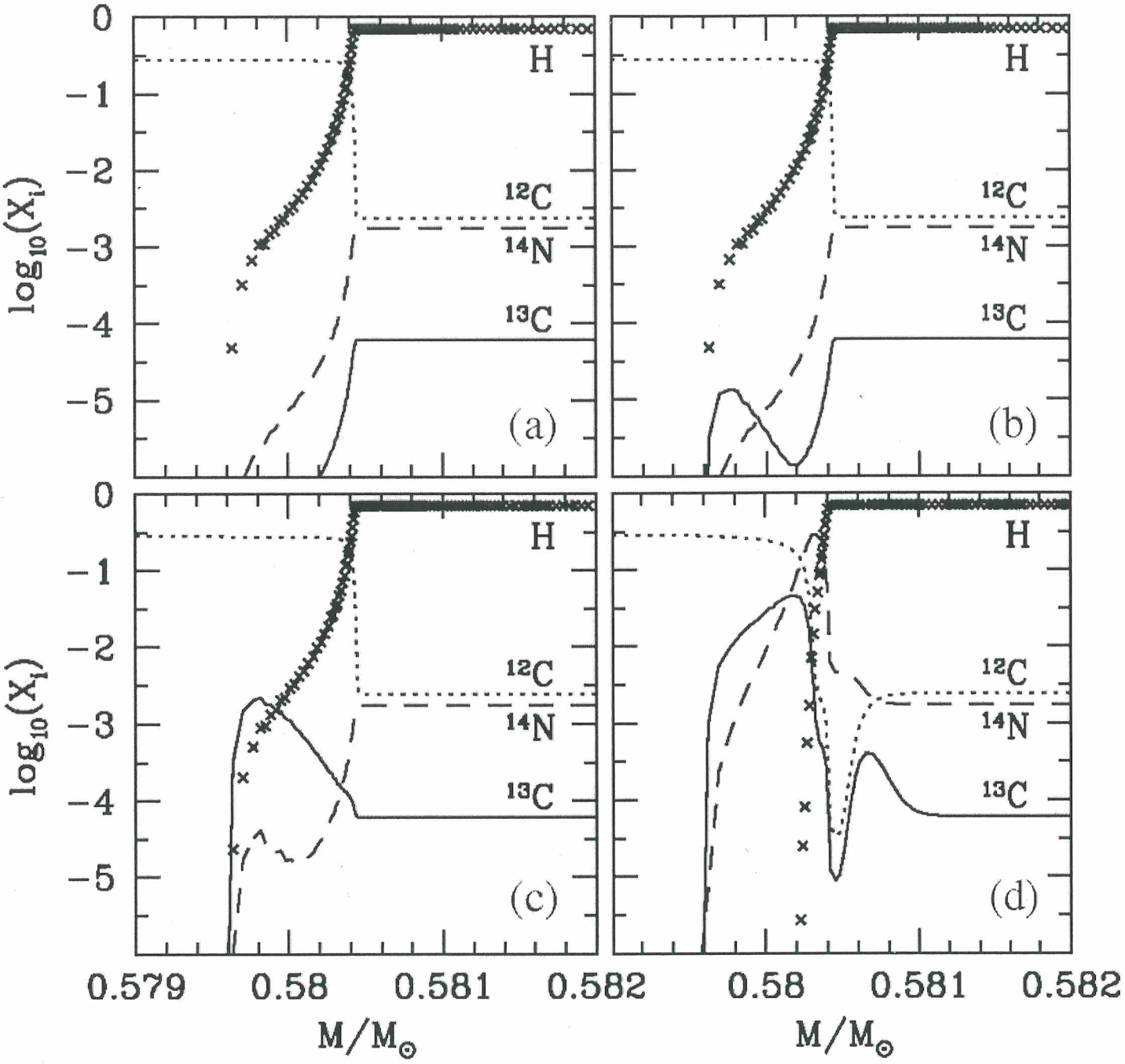

The formation of the ^{13}C pocket according to Straniero *et al.* (2009). The sequence of the panels shows the evolution of the chemical composition in the transition zone between the H-rich envelope and the H-exhausted core. The various lines represent the abundances of H (crosses), ^{12}C (dotted), ^{13}C (solid), and ^{14}N (dashed). (a) The TDU just occurred and the convective envelope is receding. (b) Production of ^{13}C by proton capture on the abundant ^{12}C starts in the hotter region. (c) Some ^{14}N is also produced, and (d) the ^{13}C (and ^{14}N) pocket is fully developed.

THEORY vs OBSERVATIONS

- AGB 'in situ' CHALLENGING.

  e.g. CARBON STARS

  ABIA et al. 2002 ApJ 579 817

  & LOW METALLICITY

- EXTRINSIC s† STARS

  - POST AGB
  - Ba II / BINARIES

SPECTRUM of CARBON (AGB) STAR in region 'minimally' affected by molecular bands

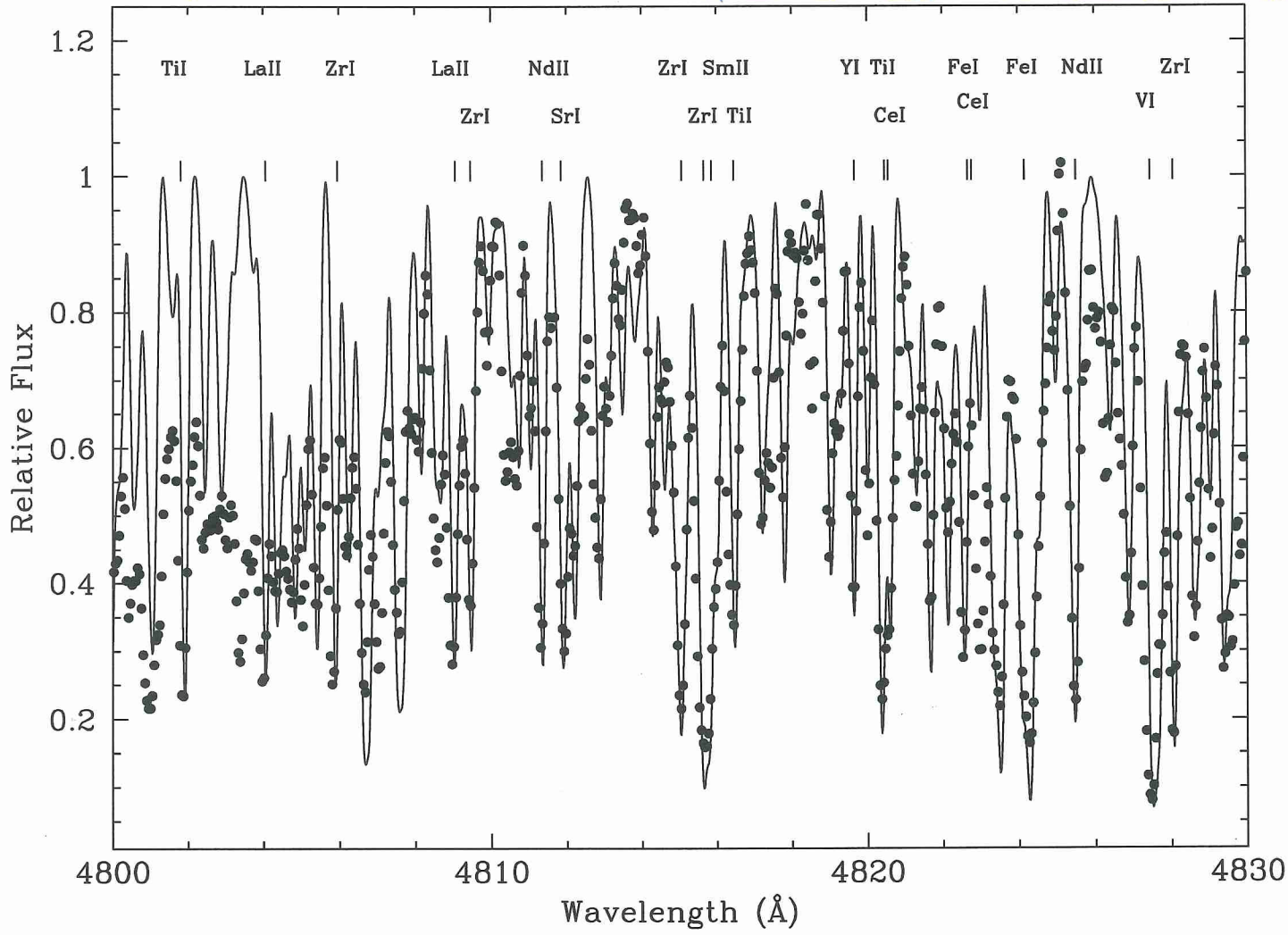

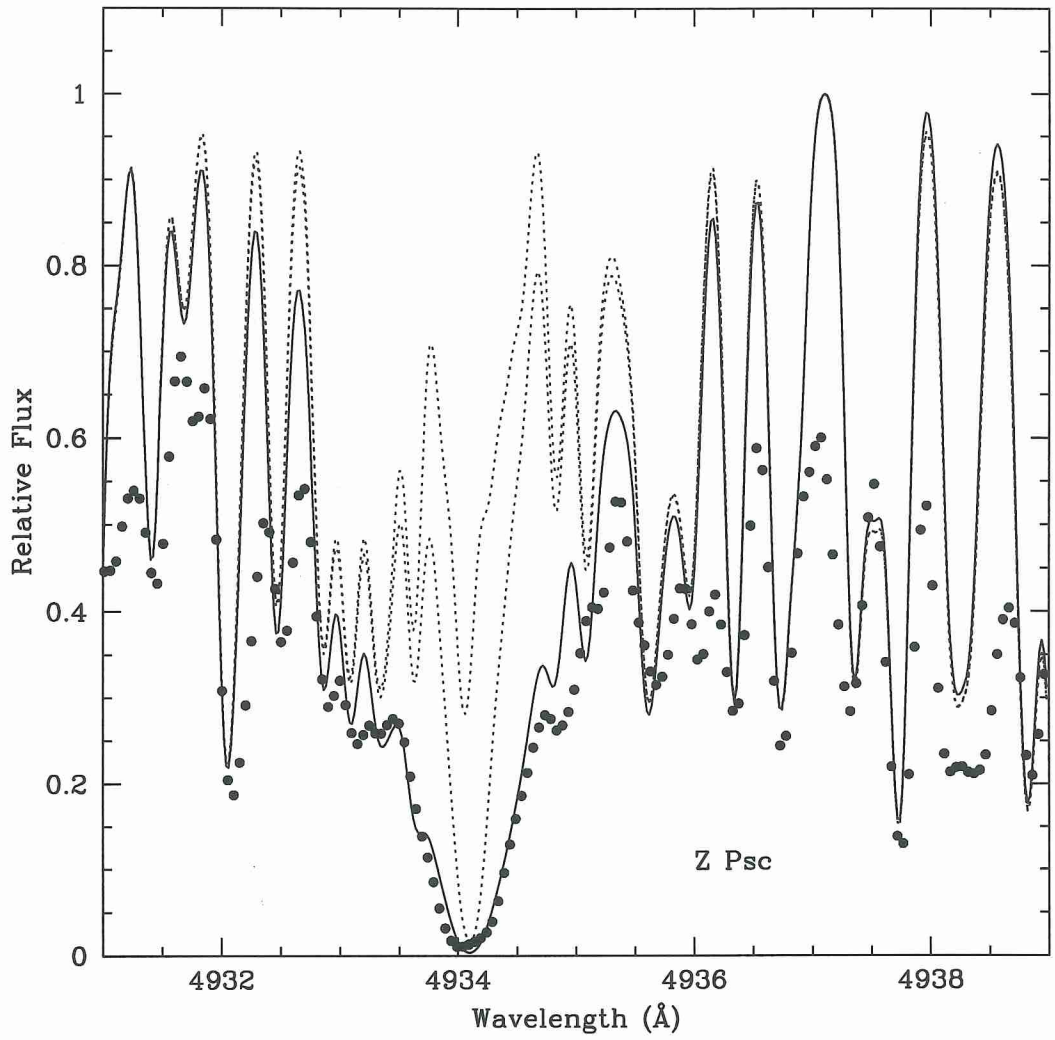

log Ba = 3.1

2.13

—00

CARBON STAR

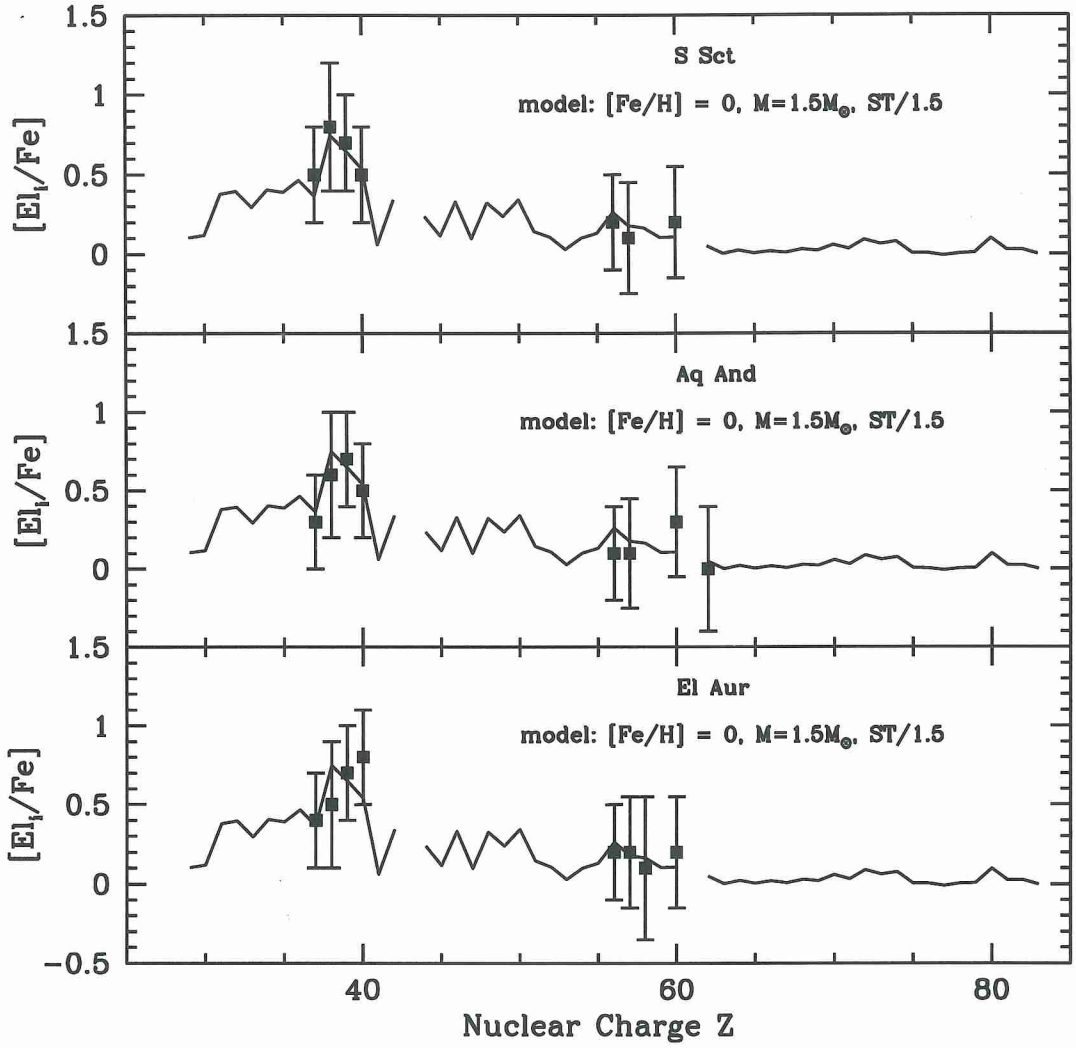
S Sct
model: [Fe/H] = 0, M=1.5M⊙, ST/1.5
Aq And
model: [Fe/H] = 0, M=1.5M⊙, ST/1.5
El Aur
model: [Fe/H] = 0, M=1.5M⊙, ST/1.5
[El/Fe]
1.5
1
0.5
0
−0.5
40
60
80
Nuclear Charge Z

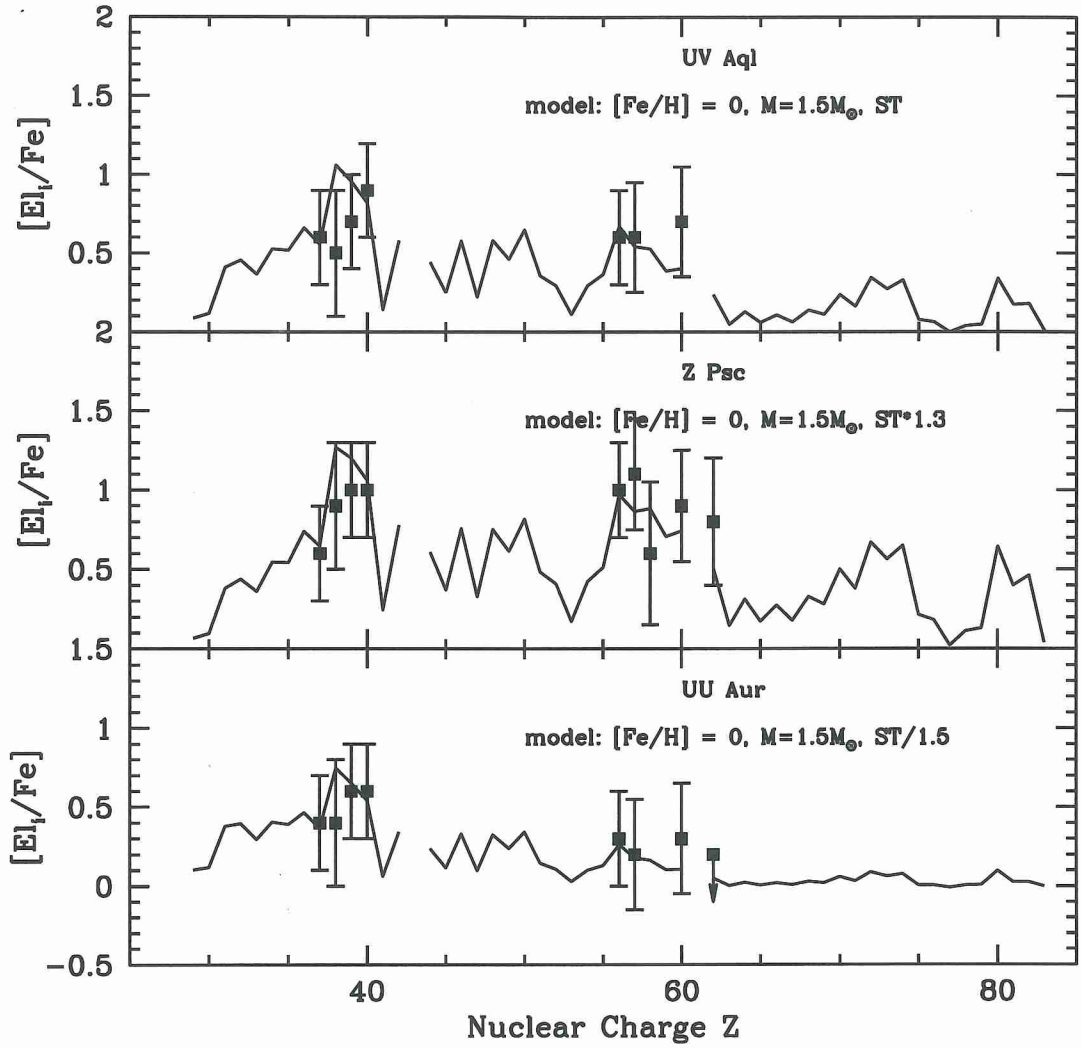
UV Aql
model: [Fe/H] = 0, M=1.5M⊙, ST
Z Psc
model: [Fe/H] = 0, M=1.5M⊙, ST*1.3
UU Aur
model: [Fe/H] = 0, M=1.5M⊙, ST/1.5
[El_i/Fe]
Nuclear Charge Z
40
60
80

THEORY as FeH VARIES

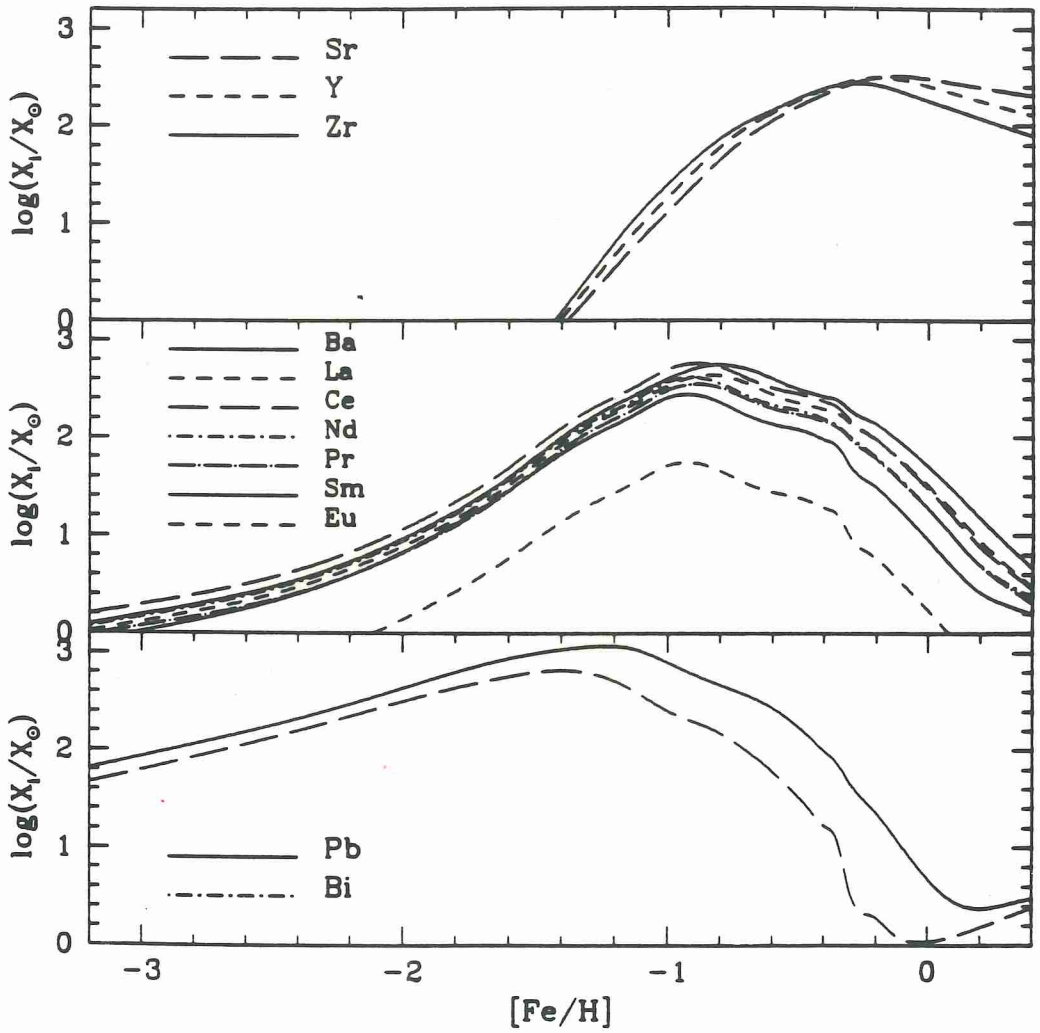

TORINO MODELS (BUSSO, GALLINO ...)

LOW MASS : $^{13}C(\alpha,n)^{16}O$

FIXED ^{13}C mass

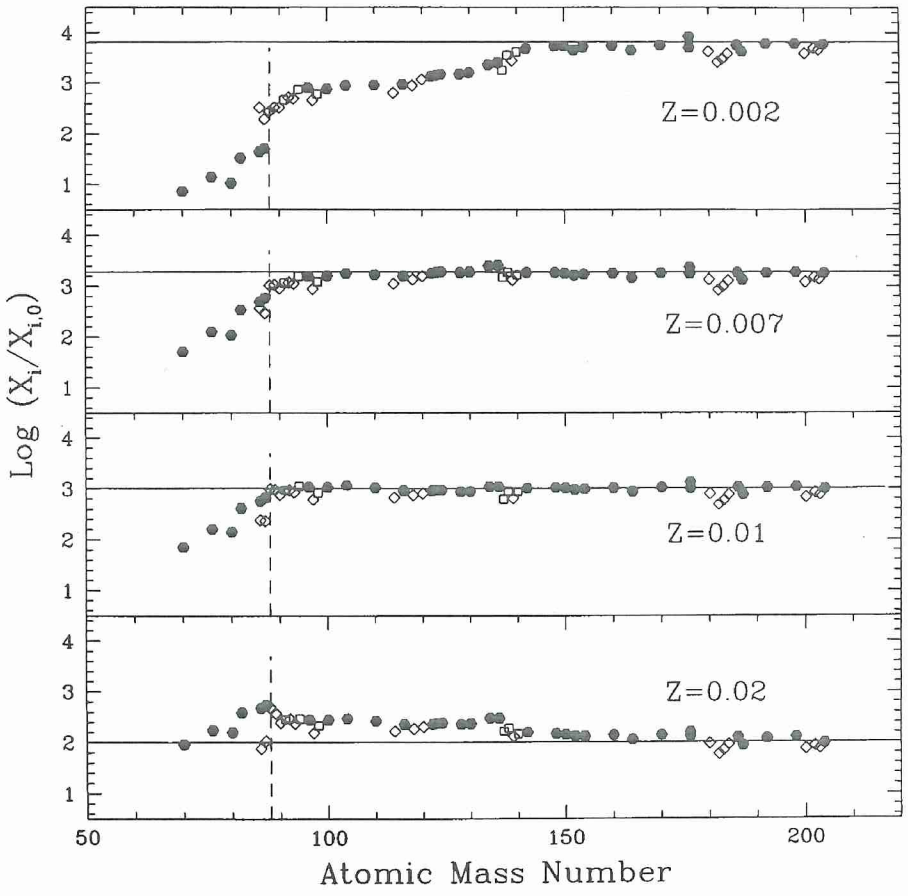

Figure 13 Distributions of enhancement factors of neutron-rich slow neutron capture (*s*)-process isotopes compared with the initial composition for different *Z* values in the material cumulatively mixed to the surface of thermal-pulse–asymptotic giant branch stars. The *horizontal line* through Bi is drawn as a guide to the eye. Models are for a 2-$M_\odot$ star, run at different metallicities, with the same standard (*ST*) choice of the ^{13}C pocket. *Heavy dots* represent *s*-only nuclei; *open squares* are nuclei that are at least 80% *s* process; *open diamonds* are nuclei with *s* contributions between 60% and 80%. For decreasing *Z*, progressively heavier nuclei are favored. In the range of $Z = (1/2\text{–}1/3) \times Z_\odot$ the distribution is relatively flat, and $Z = 0.01$ is a good approximation of the solar system main component. Note that the results are dependent on the ^{13}C pocket amount and inversely proportional to *Z*. For example, a case with $Z = 0.01$ and a ^{13}C pocket 1/2 of the ST value would be indistinguishable from that of the bottom panel.

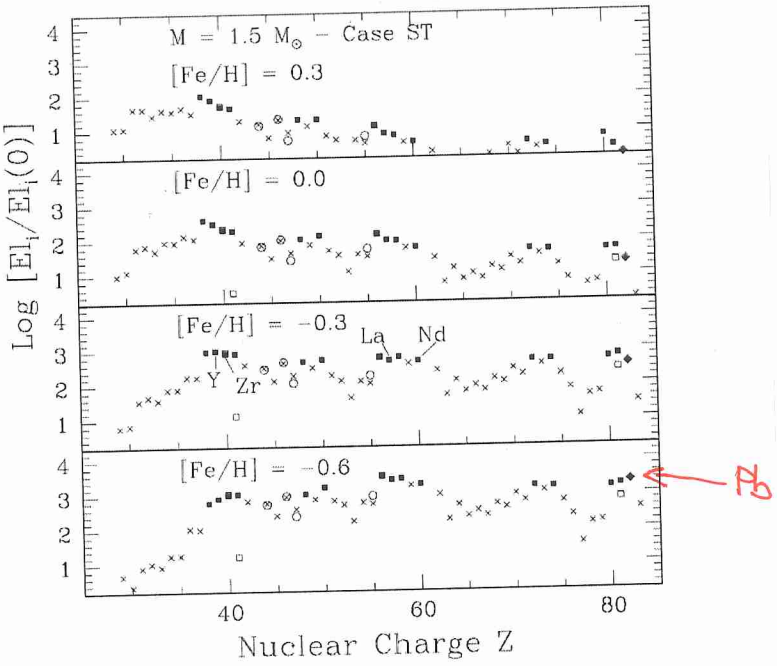

FIG. 1.—Distribution of the elements from Cu to Bi in the He intershell as a function of the initial metallicity. The elements mainly produced by the main component of the *s*-process (by at least 50% according to Arlandini et al. 1999) are shown as filled squares. Pb has a special symbol (*filled diamond*) because it is mainly attributed to the strong *s*-process component deriving from AGB stars of low metallicity (Travaglio et al. 2001). The models refer to a 1.5 $M_\odot$ star, with the choice ST for the ^{13}C pocket discussed in the text, and with metallicities from [Fe/H] = 0.3 down to −0.6. For elements affected by the decay of unstable isotopes whose half-life is longer than a typical interpulse period but shorter than 10^9 yr, open symbols refer to abundances before decay.

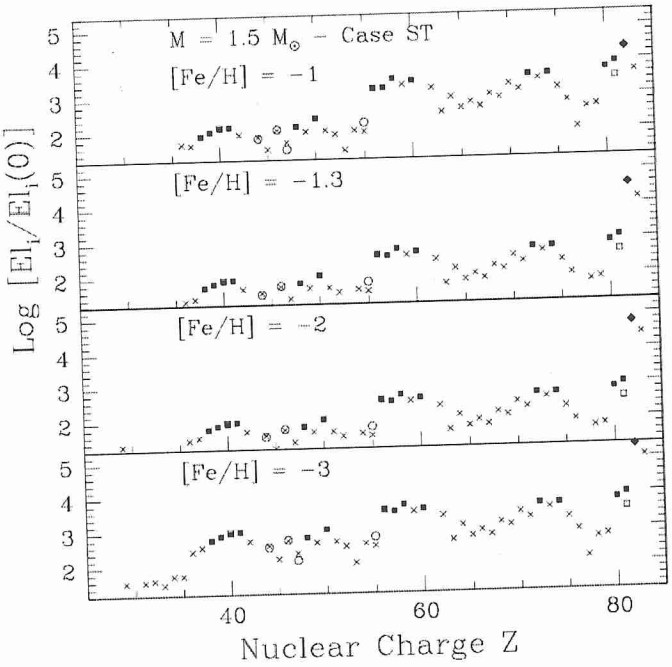

FIG. 2.—Same as Fig. 1, but for metallicities from [Fe/H] = −1 down to [Fe/H] = −3.

CH STARS

(mass transfer)

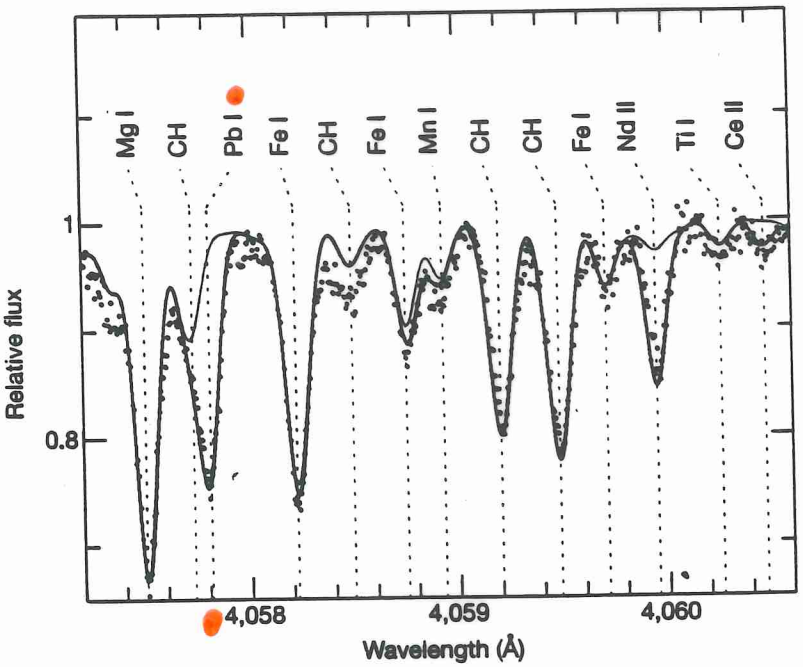

Figure 1 Comparison between observed and synthetic spectra of HD 196944 around the Pb I line at 405.781 nm. The observed spectrum (dots) has been obtained at the ESO 3.6-m telescope and Coudé Echelle Spectrometer delivering a spectral resolution $\lambda/\Delta\lambda$ of 135,000 at 405 nm. Synthetic spectra corresponding to [s/Fe] = 0 (thin solid line; in this case the Pb line is not visible) and [s/Fe] given in Table 1 (thick solid line) are also shown.

[Fe/H] = −2.45

VAN ECK et al. (2001)

[Fe/H]

-2.45

-1.65

-1.7

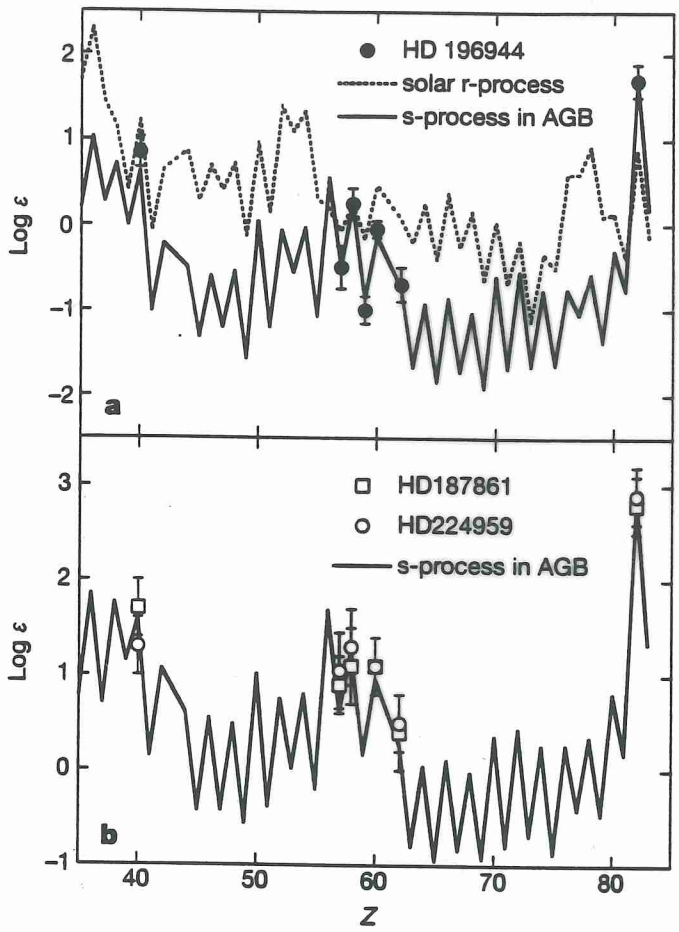

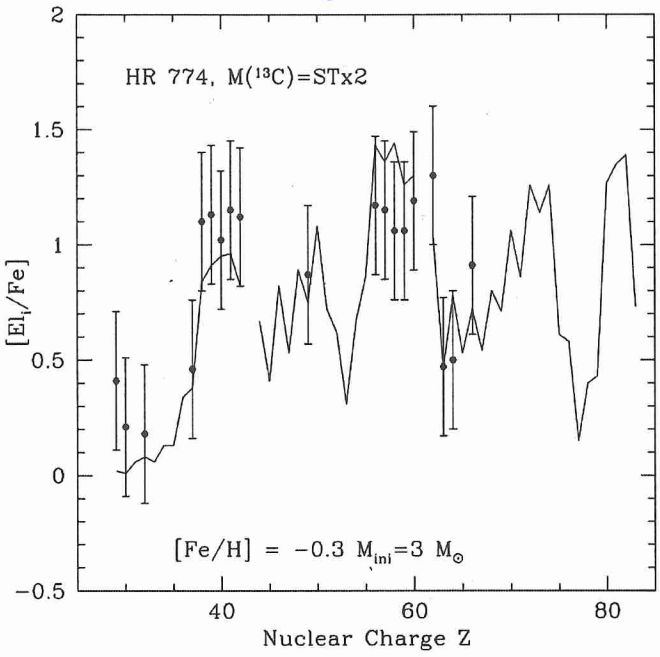

FIG. 13*a*

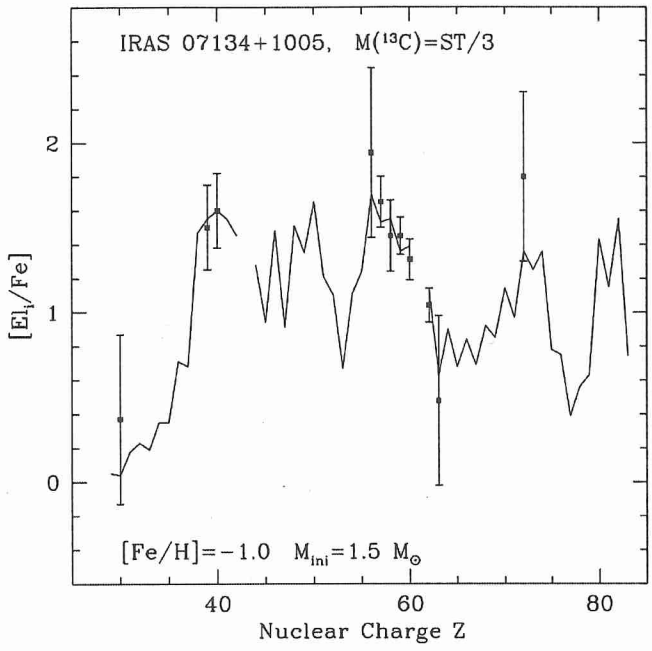

FIG. 13*b*

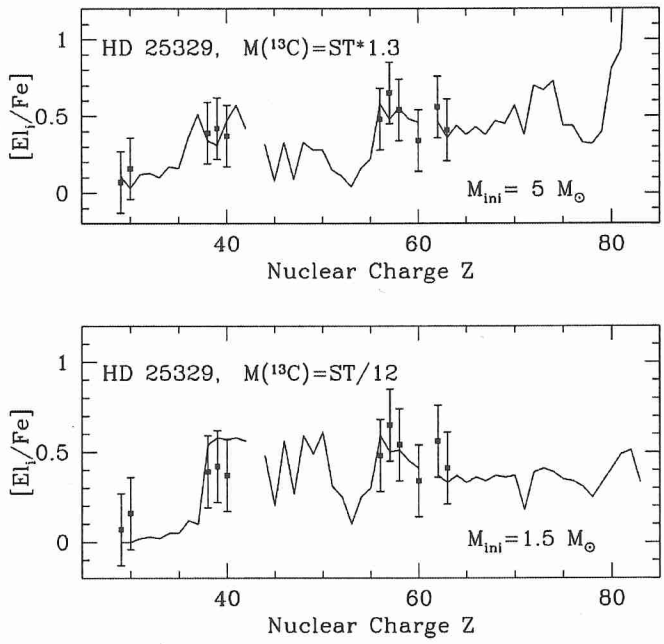

FIG. 13*c*

FIG. 13.—(*a*) Detailed reproduction of the observed abundances for the classical Ba II giant HR 774. Observations are from Smith (1984) and Tomkin & Lambert (1983) as compiled in Paper II. See text for details. (*b*) Detailed reproduction of the observed abundances for the post-AGB supergiant IRAS 07134+1005. Observations are from Van Winckel & Reyniers (2000). See text for details. (*c*). Two attempts at reproducing the observed data for the Population II *s*-enriched dwarf HD 25329 performed with an LMS and an IMS model. Observations are from Beveridge & Sneden (1994). See text for details.

different mass transfer approaches. One assumes a single phenomenon of accretion, at the 20th TP, with a dilution of 0.2 (i.e., one part of the AGB envelope per five parts of the atmosphere of the secondary component). The second assumes a continuous process, up to the 20th pulse, and yields a dilution of 0.4. Because of the uncertainties of mass-loss rates and our poor knowledge of how and when mass transfer phenomena occur, we do not claim that these are the only or even the best solutions. They, however, indicate that a moderately massive primary component is necessary here. In this way, we reach an agreement also for the carbon abundance (values of [C/Fe] in the 0.5–0.7 range can be obtained, depending on the assumptions made, to be compared with the 0.7 ± 0.1 observation). We found this datum difficult to reproduce otherwise.

4.2. *IRAS 07134+1005: A Post-AGB Supergiant*

This star belongs to the group of supergiants showing the 21 μm feature in their mid-infrared spectra, which is suspected to derive from C-rich compounds (Kwok, Volk,